synthesized from the analogous doubly bridged red-brown complex by chlorine oxidation as described above.

Registry No. $[NH_3(tren)CoO_2Co(tren)NH_3](ClO_4)_4$, 37480-75-4; $[NH_3(tren)CoO_2Co(tren)NH_3](NO_3)_4$, 37480-76-5; $[NH_3(tren)CoO_2Co(tren)NH_3]Cl_4 \cdot 2H_2O$, 37475-77-7; $[NH_3(tren)CoO_2Co(tren)NH_3]Br_4$, 37480-77-6; $[NH_3(tren)CoO_2Co(tren)NH_3]I_4$, 37480-78-7; $[py(tren)CoO_2Co(tren)py]I_4 \cdot H_2O$, 37475-78-8; $[(tren)Co(O_2,OH)Co(tren)](ClO_4)_3$, 37480-79-8; $[(tren)Co(O_2,NH_2)Co(tren)]I_3$, 37480-74-3; $[(tren)Co(O_2,NH_2)Co(tren)](ClO_4)_3 \cdot H_2O$, 37475-76-6; $[NH_3(tren)CoO_2Co(tren)NH_3](ClO_4)_5 \cdot 2H_2O$, 37189-79-0; $[tren\ Co(O_2,NH_2)Co(tren)](ClO_4)_4 \cdot 2H_2O$, 37189-77-8; $[H_2O(tren)CoO_2Co(tren)H_2O](ClO_4)_5$, 37189-78-9.

Acknowledgment. We thank Dow Chemical Co., Midland, Mich., for the gift of tris(2-aminoethyl)amine.

Contribution from the Department of Chemistry and Geology, Clemson University, South Carolina 29631

Absolute Configuration of Coordination Compounds. I. Nickel(II) and Zinc(II) Complexes of PAPY[1]

V. A. FISHMAN and J. F. GELDARD*

Received July 31, 1972

Exciton theory has been used to interpret the circular dichroism and visible spectra of the nickel(II) and zinc(II) complexes of PAPY. Excellent qualitative agreement between the observed and calculated spectra has enabled an assignment of absolute configuration for these complexes. The quantitative disagreement in line position is discussed in terms of the approximations involved in the theory.

Introduction

Recently, there has been considerable interest in the determination of the absolute configuration of coordination complexes by analysis of their circular dichroism (CD) spectra within the framework of the exciton theory.[2-10] The theory allows for coupling between free ligand transitions upon formation of a complex. The coupling arises from electrostatic interactions between the various transition dipole moments associated with the ligand transitions.

Transitions of the coordinated ligands can then be expressed as functions of those of the free ligands, and from a knowledge of these latter, one can deduce the signs of the CD bands for such transitions. Thus, the stereochemistry of a given optical isomer is determined by comparison of the observed and calculated CD spectra. This application of the theory gives qualitatively sound results although quantitative errors arise from the approximations inherent in the method.[11,12] The theory has been most commonly applied to tris-bidentate chelate complexes. In this paper, we apply the exciton method in bis-tridentate chelate complexes. Specifically, we assign the absolute configurations of the two complexes bis(1-(2′-pyridyl)-3-(6″-methyl-2″-pyridyl)-1,2-diaza-2-propenato)nickel(II) and bis(1-(2′-pyridyl)-3-(6″-methyl-2″-pyridyl)-1,2-diaza-2-propenato)-zinc(II), complexes I and II, respectively.

Theory and Theoretical Results

The quantum mechanical formulation of optical activity by Rosenfeld[13] leads to analytical expressions for the rotational strength R_{ba} of a molecular electronic transition from state $|a\rangle$ to state $|b\rangle$ and for the rotatory parameter β_a appropriate to molecules in state $|a\rangle$

$$R_{ba} = \mathrm{Im}\{\langle a|\vec{\mu}_e|b\rangle \cdot \langle b|\vec{\mu}_m|a\rangle\}$$

$$\beta_a = \frac{c}{3\pi h}\sum_b R_{ba}/(\upsilon_{ba}^2 - \upsilon^2)$$

where $\vec{\mu}_e$ and $\vec{\mu}_m$ are the electric and magnetic dipole moment operators, respectively, and υ_{ba} is the frequency of excitation from state $|a\rangle$ to $|b\rangle$.

The exciton formulation of Moffitt[14] and Frenkel[15] allows the expression of the ground-state wave function of a bis-tridentate chelate complex, $|C_0\rangle$, as a product of the individually antisymmetrized ground-state wave functions of the two ligands, $|X_0\rangle$ and $|Y_0\rangle$, and the metal, $|M_0\rangle$: $|C_0\rangle = |X_0Y_0M_0\rangle$. Furthermore, certain of the excited states of the complex may be approximated by product functions involving only excited states of the ligands, the metal ion being represented by its ground-state wave function. Typically, corresponding to the ith excited state of the ligand X is an excited state of the complex, say the jth; the two states are related by $|C_j\rangle = |X_iY_0M_0\rangle$. It is to be noted that this formulation precludes electron exchange between the ligands and the metal and assumes no change in ligand geometry upon complexation. In the complexes reported here, ligands X and Y are identical and exhibit a broad absorption

(1) The deprotonated form of the tridentate chelating agent 1-(2′-pyridyl)-3-(6″-methyl-2″-pyridyl)-1,2-diaza-2-propene.
(2) (a) A. J. McCaffery, S. F. Mason, and R. E. Ballard, *J. Chem. Soc.*, 2883 (1965); (b) C. J. Hawkins and E. Larsen, *Acta Chem. Scand.*, 19, 1969 (1965).
(3) A. J. McCaffery and S. F. Mason, *Proc. Chem. Soc., London*, 211 (1963).
(4) A. J. McCaffery, S. F. Mason, and B. J. Norman, *Proc. Chem. Soc., London*, 259 (1964).
(5) E. Larsen, S. F. Mason, and G. H. Searle, *Acta Chem. Scand.*, 20, 191 (1966).
(6) J. Mason and S. F. Mason, *Tetrahedron*, 23, 1919 (1967).
(7) B. Bosnich, *Inorg. Chem.*, 7, 178 (1968).
(8) S. F. Mason and B. J. Norman, *Inorg. Nucl. Chem. Lett.*, 3, 285 (1967).
(9) S. F. Mason and B. J. Norman, *Chem. Phys. Lett.*, 2, 22 (1968).
(10) J. Ferguson, C. J. Hawkins, N. A. P. Kane-Maguire, and H. Lip, *Inorg. Chem.*, 8, 771 (1969).
(11) A. J. McCaffery, S. F. Mason, and B. J. Norman, *J. Chem. Soc. A*, 1428 (1969).
(12) S. F. Mason and B. J. Norman, *J. Chem. Soc. A*, 1442 (1969).
(13) L. Rosenfeld, *Z. Phys.*, 52, 161 (1928).
(14) W. Moffitt, *J. Chem. Phys.*, 25, 467 (1956).
(15) J. Frenkel, *Phys. Rev.*, 37, 17 (1931).

in the range 19-25 kK. We associate two excited states, $|X_1\rangle$ and $|X_2\rangle$, with the two transitions responsible for this absorption in ligand X, with corresponding designations for ligand Y. A basis for the calculation of the excited-state wave functions of the complex corresponding to the four free-ligand excited states is written

$$\Phi = \begin{pmatrix} |C_1\rangle \\ |C_2\rangle \\ |C_3\rangle \\ |C_4\rangle \end{pmatrix} = \begin{pmatrix} |X_1Y_0M_0\rangle \\ |X_2Y_0M_0\rangle \\ |X_0Y_1M_0\rangle \\ |X_0Y_2M_0\rangle \end{pmatrix}$$

The structure assumed for the anionic form of the ligands is shown in Figure 1. The complex belongs to the C_2 point symmetry group, the geometry of the enantiomer used for the present discussion being shown in Figure 2. We write for the Hamiltonian of the complex, $\hat{h}_c$

$$\hat{h}_c = \hat{h}_x + \hat{h}_y + V_{xy}$$

where $\hat{h}_x$ and $\hat{h}_y$ are the free-ligand Hamiltonians and V_{xy} is the Coulomb interaction between electronic distributions on ligands X and Y. Because the four excited-state basis functions span the irreducible representations A and B twice each, we block-diagonalize $\mathbf{H}^\Phi$ by an arbitrary choice of symmetry functions; this facilitates the use of general expressions for the quantities of interest. These symmetry functions are designated by Ω; the Hamiltonian in this basis is

$$\mathbf{H}^\Omega = \begin{pmatrix} \Delta\epsilon_1 + V_{13} & V_{14} & 0 & 0 \\ V_{14} & \Delta\epsilon_2 + V_{24} & 0 & 0 \\ 0 & 0 & \Delta\epsilon_1 - V_{13} & -V_{14} \\ 0 & 0 & -V_{14} & \Delta\epsilon_2 - V_{24} \end{pmatrix}$$

where $V_{ij} = \langle X_iY_0|V_{xy}|X_0Y_j\rangle$ and $\Delta\epsilon_1$ and $\Delta\epsilon_2$ are the energies of the transitions $|0\rangle \rightarrow |1\rangle$ and $|0\rangle \rightarrow |2\rangle$, respectively, for ligands X and Y, the eigenvalues now being relative to the ground-state energy of the complex. In transforming $\mathbf{H}^\Phi$ to $\mathbf{H}^\Omega$, we have arbitrarily set $H\phi_{12}$ equal to zero. The implications of this approximation and of others involved in this method are discussed below.

The eigenvalues are

$$\lambda_\pm{}^A = \frac{1}{2}[\Delta\epsilon_1 + \Delta\epsilon_2 + V_{13} + V_{24} \pm \{(\Delta\epsilon_1 - \Delta\epsilon_2 + V_{13} - V_{24})^2 + 4V_{14}{}^2\}^{1/2}]$$

$$\lambda_\pm{}^B = \frac{1}{2}[\Delta\epsilon_1 + \Delta\epsilon_2 - V_{13} - V_{24} \pm \{(\Delta\epsilon_1 - \Delta\epsilon_2 - V_{13} + V_{24})^2 + 4V_{14}{}^2\}^{1/2}]$$

and the correct symmetry functions, Ψ, are given by

$$\Psi = \frac{1}{\sqrt{2}} \begin{pmatrix} \sin\alpha & \cos\alpha & \sin\alpha & \cos\alpha \\ \cos\alpha & -\sin\alpha & \cos\alpha & -\sin\alpha \\ \sin\beta & \cos\beta & -\sin\beta & -\cos\beta \\ \cos\beta & -\sin\beta & -\cos\beta & \sin\beta \end{pmatrix} \Phi$$

where $\tan 2\alpha = -2V_{14}/(\Delta\epsilon_1 - \Delta\epsilon_2 + V_{13} - V_{24})$ and $\tan 2\beta = -2V_{14}/(\Delta\epsilon_1 - \Delta\epsilon_2 - V_{13} + V_{24})$. We designate by A_+ the excited state with energy $\lambda_+{}^A$, etc. The general expressions for the dipole strengths and rotational strengths associated with each transition in the complex are shown in Table I. The V_{ij} are evaluated by means of the dipole-dipole interaction term

$$V_{ij} = \frac{1}{d_{ij}{}^3}\left\{\vec{\rho}_i\cdot\vec{\rho}_j - \frac{3(\vec{\rho}_i\cdot\vec{d}_{ij})(\vec{\rho}_j\cdot\vec{d}_{ij})}{\vec{d}_{ij}\cdot\vec{d}_{ij}}\right\}$$

where the free-ligand transition dipole moments, $\vec{\rho}_i$ and $\vec{\rho}_j$,

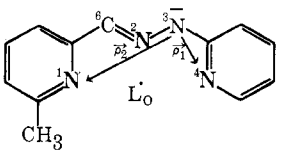

Figure 1. The idealized structure of PAPY, showing the assumed directions and relative magnitudes of the transition dipole moments, $\vec{\rho}_1$ and $\vec{\rho}_2$. Small numerical prefixes designate atoms referred to in the text.

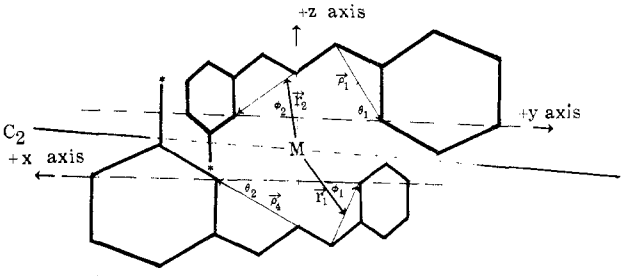

Figure 2. The geometry of complexes I and II used for the calculation of the dipole and rotational strengths and designated as the R configuration (see Appendix). $\vec{\rho}_1$ and $\vec{\rho}_2$ are the two transition moments for the one ligand; $\vec{\rho}_3$ and $\vec{\rho}_4$, those for the other. The vectors $\vec{r}_1$ and $\vec{r}_2$ mark the location of the centers of these moments and intersect the x or y axis at angles ϕ_1 or ϕ_2. The transition moments intersect the x or y axis at angles θ_1 or θ_2.

Table I. General Expressions[a] for the Dipole and Rotational Strengths of the Transition $|0\rangle \rightarrow |\Gamma\rangle$

Γ	D_{Γ_0}	R_{Γ_0}
B_-	$(\rho_1 \cos\theta_1 \sin\beta + \rho_2 \cos\theta_2 \cos\beta)^2 + 2(-\rho_1 \sin\beta \sin\theta_1 + \rho_2 \cos\beta \sin\theta_2)^2$	$\pi\{-\rho_1{}^2\bar{\nu}_1 r_1 \sin^2\beta \cos\theta_1 \sin(\phi_1 + \theta_1) - \rho_1\rho_2 \cos\beta \sin\beta \times [\bar{\nu}_1 r_1 \cos\theta_2 \sin(\phi_1 + \theta_1) + \bar{\nu}_2 r_2 \cos\theta_1 \sin(\phi_2 + \theta_2)] - \rho_2{}^2\bar{\nu}_2 r_2 \cos^2\beta \cos\theta_2 \sin(\phi_2 + \theta_2)\}$
A_-	$(\rho_1 \sin\alpha \cos\theta_1 + \rho_2 \cos\alpha \cos\theta_2)^2$	$\pi\{\rho_1{}^2\bar{\nu}_1 r_1 \sin^2\alpha \cos\theta_1 \sin(\phi_1 + \theta_1) + \rho_1\rho_2 \cos\alpha \sin\alpha \times [\bar{\nu}_1 r_1 \cos\theta_2 \sin(\phi_1 + \theta_1) + \bar{\nu}_2 r_2 \cos\theta_1 \sin(\phi_2 + \theta_2)] + \rho_2{}^2\bar{\nu}_2 r_2 \cos^2\alpha \cos\theta \sin(\phi_2 + \theta_2)\}$
B_+	$(\rho_1 \cos\theta_1 \cos\beta - \rho_2 \cos\theta_2 \sin\beta)^2 + 2(\rho_1 \cos\beta \sin\theta_1 + \rho_2 \sin\beta \sin\theta_2)^2$	$\pi\{-\rho_1{}^2\bar{\nu}_1 r_1 \cos^2\beta \cos\theta_1 \sin(\phi_1 + \theta_1) + \rho_1\rho_2 \cos\beta \sin\beta \times [\bar{\nu}_1 r_1 \cos\theta_2 \sin(\phi_1 + \theta_1) + \bar{\nu}_2 r_2 \cos\theta_1 \sin(\phi_2 + \theta_2)] - \rho_2{}^2\bar{\nu}_2 r_2 \sin^2\beta \cos\theta_2 \sin(\phi_2 + \theta_2)\}$
A_+	$(\rho_1 \cos\alpha \cos\theta_1 - \rho_2 \sin\alpha \cos\theta_2)^2$	$\pi\{\rho_1{}^2\bar{\nu}_1 r_1 \cos^2\alpha \cos\theta_1 \sin(\phi_1 + \theta_1) - \rho_1\rho_2 \cos\alpha \sin\alpha \times [\bar{\nu}_1 r_1 \cos\theta_2 \sin(\phi_1 + \theta_1) + \bar{\nu}_2 r_2 \cos\theta_1 \sin(\phi_2 + \theta_2)] + \rho_2{}^2\bar{\nu}_2 r_2 \sin^2\alpha \cos\theta_2 \sin(\phi_2 + \theta_2)\}$

[a] The angle factors ϕ and θ are defined in Figure 2.

are given by $\vec{\rho}_k = \langle k|\vec{\mu}_e|0\rangle$, $\vec{\mu}_e$ being as before the electric dipole moment operator, and d_{ij} is the distance between their centers. The dipole strengths and rotational strengths were calculated from the formulas[16]

$$D_k = \sum_i\sum_j C_{ik}C_{jk}\vec{\bar{\rho}}_i\cdot\vec{\bar{\rho}}_j$$

$$R_k = \Pi\sum_i\sum_j C_{ik}C_{jk}\bar{\nu}_j\vec{\bar{\rho}}_i\cdot(\vec{\bar{r}}_j \times \vec{\bar{\rho}}_j)$$

where the sum is over the excited states of the complex, $\vec{r}_j$ is

(16) B. Bosnich, *Accounts Chem. Res.*, 2, 266 (1959).

Table II. Hueckel Molecular Orbital Results[a]

Parameters										
α_N	$\alpha_{N'}$[b]	β_{CN}[c]	$\beta_{CN'}$[d]	$\beta_{NN'}$[e]	Transition $\pi \rightarrow \pi^*$	Energy,[f] kK	Transition ρ_x	Dipole ρ_y	Moment[g] $\lvert\rho\rvert$	Dipole strength[h]
0.2	2.0	1.5	1.0	1.0	8 → 9	22.7	−7.69	−2.35	8.05	64.74
					8 → 10	26.1	+4.47	−1.81	4.82	23.28
0.2	2.5	1.5	1.0	1.0	8 → 9	22.7	−5.93	−2.23	6.34	40.12
					8 → 10	25.9	+4.40	−1.56	4.70	22.10
0.1	1.5	1.5	1.0	1.0	8 → 9	22.7	−10.34	−2.09	10.31	10.61
					8 → 10	26.2	+3.82	−2.11	4.36	18.96
0.1	2.0	1.5	1.0	1.0	8 → 9	22.7	−7.93	−2.19	8.23	67.76
					8 → 10	25.9	+4.31	−1.84	4.68	21.96

[a] Although all states transform as the A'' representation of the C_s point symmetry group, no configuration interaction has been included in these calculations. [b] α_N and $\alpha_{N'}$ are the Coulomb integrals for N1, N2, and N4 and for N3, respectively. [c] Carbon to N1, N2, and N4 resonance integral. [d] Carbon to N3 resonance integral. [e] N2 to N3 resonance integral. [f] $\pi_8 \rightarrow \pi_9$ transition energy is set equal to 22.7 kK and all others are calculated by proportion. [g] x and y components defined by Figure 1 in 10^{-18} cgsu and the magnitude of the resultant. [h] 10^{-36} cgsu. Both the transition moment and dipole strength values include the orbital degeneracy factor.

the position vector of the center of the jth transition moment, $\vec{\rho}_j$, $\bar{\nu}_j$ is the energy of the transition $|0\rangle \rightarrow |j\rangle$ expressed in wave numbers, and the C_{lm} are the appropriate mixing coefficients.

The calculation of the energies, rotational strengths, and dipole strengths of the transitions of the complex, and thus the prediction of the visible and CD spectra, ultimately depends upon the values assigned the free-ligand transition energies ($\Delta\epsilon_1$ and $\Delta\epsilon_2$), the magnitudes and directions of the corresponding transition dipole moments ($\vec{\rho}_1$ and $\vec{\rho}_2$), and the structure assumed for the complex. The magnitudes of $\Delta\epsilon_1$, and $\Delta\epsilon_2$, ρ_1, and ρ_2 were obtained empirically by Gauss-Newton (GN) nonlinear analysis of the visible spectrum of the free ligand. The directions of ρ_1 and ρ_2 were initially assigned on the basis of valence-bond representations of the excited-state structures arising from charge transfer into the two dissimilar pyridine rings.

Hueckel molecular orbital (HMO) calculations were used to confirm these assignments. The results of these calculations are shown in Table II. Parameters for the nonzero matrix elements occurring in the HMO formalism were handled in standard ways.[17] Transition dipole moments were calculated from a formula that follows from the rigorous one by the assumption of zero-differential overlap[18]

$$\vec{\rho}_{jk} = \sum_p C_{jp} C_{kp} \vec{r}_p$$

for the transition $|k\rangle \rightarrow |j\rangle$. In this expression, the summation extends over the position vectors, $\vec{r}_p$, of all atoms contributing to the π-electron system, C_{jp} being the contribution of the pth atom to the jth molecular orbital.

Several sets of acceptable values were obtained for the parameters by GN analysis. All credible ones were used in the calculation outlined above. The best sets of free-ligand parameters generally gave the best agreement between observed and calculated visible and CD spectra.

The results of these calculations may be summarized as follows. The excited states are, in order of increasing energy B_-, A_-, $B_+ \approx A_+$. The dipole strengths of the four transitions from the ground state to each of these excited states fall in the order $D_{B_-} > D_{B_+} > D_{A_+} > D_{A_-}$; the rotational strengths fall in the order $R_{A_-} > R_{B_-} \gg R_{B_+} \approx R_{A_+}$. The line shapes of the visible and CD spectra are in excellent agreement with the observed. The calculated and observed transition energies differ by 1 kK; the source of this error is discussed below. Numerical values for the above

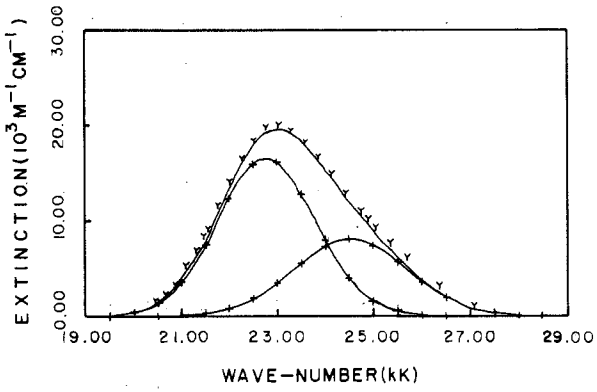

Figure 3. The visible spectrum of the ligand PAPY in ethanolic solution is represented by the points (marked as Y) used in the GN analysis. The result of a two peak GN analysis of the spectrum is shown by the crossed lines and the sum of the two peaks by the solid line.

quantities, calculated from appropriate choices for the free-ligand parameters, are shown in Table III. In only a few instances was the order of the B_- and A_- energy levels reversed. This happened when unreasonable values for the parameters were used. The predicted and observed rotational and dipole strengths are so different in these cases that we presume such results can be safely ignored.

Thus, based upon exciton analysis, the enantiomer of I or II that shows a low-energy negative CD band followed by a higher energy positive one has the absolute configuration R as shown in Figure 2. Therefore, the experimentally isolated enantiomer is the S isomer.

Discussion

Spectra. The calculation of the CD and visible spectra of complexes I and II depends upon the assignment of the magnitude and direction of the transition moments in the free ligand. As is shown in Figure 3, the ligand has a broad absorption in the range 19–25 kK, with a maximum extinction coefficient of 19,460 cm^{-1} M^{-1}. GN analysis, using symmetric gaussian line shapes, indicates the presence of two peaks in this band.

We assign the origin of these peaks to two charge-transfer (CT) bands, similar in nature but unequal in energy. Valence bond structures that are probably the major contributors to the excited configurations are shown in Figure 4. In Figure 1, the transition moments associated with these CT bands are represented by $\vec{\rho}_1$ and $\vec{\rho}_2$, with $\vec{\rho}_1$ corresponding to the high-energy transition; the centers of the two moments are located halfway along the N1–N3 and N3–N4 distances, respectively.

Table IV shows data extracted from the observed spec-

(17) A. Streitwieser, Jr., "Molecular Orbital Theory for Organic Chemists," Wiley, New York, N. Y., 1961.
(18) M. J. S. Dewar, "Molecular Orbital Theory of Organic Chemistry," McGraw-Hill, New York, N. Y., 1969.

Table III. Numerical Results for the Exciton Transition Energies, Dipole and Rotational Strengths, and Extinction Coefficients

Data set	Γ^a	ΔE,[b] kK	D_{Γ_0}[c]	R_{Γ_0}[d]	g[e]	ϵ_{Ni}	$^1/_2(\epsilon_l - \epsilon_r)$[f]	ϵ_{Zn}	$^1/_2(\epsilon_l - \epsilon_r)$[g]	$\theta_1 \mid \theta_2 \mid r_0$[h]
1	B_-	22.5	22.8	−192.8	0.85	33.2	−112	37.8	−128	60|30|0.65
	A_-	22.9	13.8	+193.4	1.40	18.9	+106	22.6	+126	
	A_+	24.7	2.4	+87.5	3.70	5.7	+84	8.5	+125	
	B_+	24.8	17.5	−88.0	0.51	11.4	−23	12.9	−26	
2	B_-	22.5	22.8	−196.0	0.86	33.0	−114	37.7	−130	
	A_-	22.9	13.8	+198.0	1.45	18.9	+109	22.6	+130	63|31|0.65
	A_+	24.7	1.7	+71.0	4.20	4.1	+68	6.0	+102	
	B_+	24.8	18.2	−73.0	0.40	11.9	−19	13.5	−22	
3	B_-	22.4	22.6	−198.8	0.88	32.7	−115	37.3	−131	
	A_-	23.0	13.7	+202.0	1.47	18.8	+111	22.4	+133	66|32|0.65
	B_+	24.7	19.1	−58.0	0.30	12.4	−15	14.1	−17	
	A_+	24.8	1.1	+54.8	4.98	2.7	+53	4.0	+79	
4	B_-	22.4	22.3	−201.0	0.90	32.2	−116	36.7	−133	
	A_-	23.0	13.5	+205.0	1.52	18.6	+113	22.2	+135	69|33|0.65
	B_+	24.7	20.0	−43.4	0.22	13.0	−11	14.8	−13	
	A_+	24.9	0.6	+39.5	6.25	1.5	+38	2.3	+57	
5	B_-	22.5	22.8	−180.4	0.79	33.1	−105	37.7	−119	
	A_-	22.9	13.9	+181.4	1.31	19.0	+100	22.7	+119	60|30|0.45
	A_+	24.6	2.4	+85.2	3.63	5.6	+82	8.4	+122	
	B_+	24.9	17.5	−86.3	0.50	11.5	−23	13.0	−26	
6	B_-	22.4	23.0	−179.7	0.78	33.2	−104	37.9	−119	
	A_-	23.0	13.7	+181.4	1.33	18.8	+100	22.4	+119	63|31|0.45
	A_+	24.7	1.8	+73.8	4.03	4.4	+71	6.5	+106	
	B_+	24.9	18.0	−75.6	0.42	11.8	−20	13.4	−22	
7	B_-	22.4	22.8	−183.1	0.80	32.9	−106	37.5	−121	
	A_-	23.1	13.7	+187.4	1.37	18.8	+103	22.4	+123	66|32|0.45
	A_+	24.7	1.2	+56.1	4.83	2.8	+54	4.2	+80	
	B_+	24.8	18.9	−60.4	0.32	12.3	−16	13.9	−18	
8	B_-	22.3	22.5	−186.0	0.83	32.4	−107	36.9	−122	
	A_-	23.1	13.5	+192.4	1.42	18.6	+106	22.3	+127	69|33|0.45
	B_+	24.7	19.8	−45.5	0.23	12.9	−12	14.6	−13	
	A_+	24.8	0.6	+39.2	6.21	1.5	+38	2.3	+56	
9	B_-	22.1	22.9	−155.4	0.68	32.7	−89	37.2	−101	
	A_-	23.3	13.8	+155.8	1.13	19.1	+87	22.9	+104	60|30|0.22
	A_+	24.5	2.5	+80.3	3.28	5.8	+77	8.7	+114	
	B_+	25.0	17.4	−80.7	0.47	11.4	−21	13.0	−24	
10	B_-	22.0	22.8	−159.8	0.70	32.4	−91	36.9	−104	
	A_-	23.4	14.1	+168.9	1.20	19.7	+94	23.5	+113	63|31|0.22
	A_+	24.6	1.4	+56.8	4.06	3.3	+54	5.0	+81	
	B_+	24.9	18.2	−66.0	0.36	12.0	−17	13.5	−20	
11	B_-	21.9	22.5	−163.7	0.73	31.8	−93	36.3	−106	
	A_-	23.4	14.2	+180.4	1.27	19.9	+101	23.7	+121	66|32|0.22
	A_+	24.7	0.6	+34.7	5.66	1.5	+33	2.2	+50	
	B_+	24.9	19.2	−51.3	0.27	12.6	−13	14.2	−15	
12	B_-	21.8	22.0	−167.0	0.76	31.0	−94	35.4	−107	
	A_-	23.5	14.0	+188.6	1.35	19.6	+106	23.5	+127	69|33|0.22
	B_+	24.8	20.3	−37.2	0.18	13.2	−10	15.0	−11	
	A_+	24.8	0.2	+15.5	10.43	0.4	+15	.5	+22	

[a] Excited-state symmetry designation. [b] Transition energy $|0\rangle \rightarrow |\Gamma\rangle$. [c] Dipole strength in 10^{-36} cgsu. [d] Rotational strength in 10^{-40} cgsu. [e] Kuhn's anisotropy factor ($\times 10^{-3}$). [f] Half the sum ($\times 10^{-3}$) and the difference of ϵ_l and ϵ_r calculated from the half-widths of data set 1 in Table VI. [g] As in footnote *f* but calculated from the half-widths of data set 2 in Table VI. [h] Values of θ_1 and θ_2 as defined in Figure 2. r_0 is the distance of the ligand origin (L_0 in Figure 1) from the metal in angstrom units.

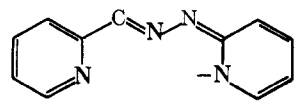

(a)

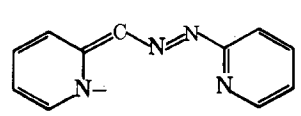

(b)

Figure 4. Valence-bond representations of the excited states of PAPY: (a) the excited state associated with the transition dipole moment $\vec{\rho}_1$; (b) that associated with $\vec{\rho}_2$. Methyl groups are not shown.

trum of the ligand by GN analysis assuming two peaks present. The best set of peak components is plotted in Figure 3, and all sets were used in the calculation of the spectra of I and II. Table V contains representative results obtained by GN analysis of the ligand spectrum assuming one and three peaks to be present. One peak is clearly inadequate and three peaks give no better description of the observed spectrum than two.

As can be seen in Figure 4, if the two transitions involve roughly equal transfer of charge, then the ratio of the transition moments should be almost the same as the ratio of the distances N1-N3 and N4-N3. This ratio, calculated from the idealized geometry shown in Figure 1, is 1.73; the ratio obtained from GN analysis is 1.36. Further support for the assignment of $\vec{\rho}_1$ and $\vec{\rho}_2$ is found in the behavior of the spectra of I and II. The maximum shows a blue shift as the dielectric constant of the solvent increases (Figure 5). This result is easily understood, given the interpretation of $\vec{\rho}_1$ and $\vec{\rho}_2$ above. Each transition brings the ligand's negative charge adjacent to the metal ion. The ground state therefore has more charge separation than the excited states and

Table IV. Peak Parameters for the Visible Spectrum of the Ligand 1-(2'-Pyridyl)-3-(6''-methyl-2''-pyridyl)-1,2-diaza-2-propene, Obtained by Gauss–Newton Nonlinear Analysis: Two-Peak Analysis

Data set	$\bar{\nu}^a$	δ^a	$\epsilon_{max}{}^a$	f^b	D^b	ρ^b	$\rho_1/\rho_2{}^b$	Area[c]	SD[d]
1	22.7	1.2	17.6	0.20	18.3	4.3	1.4	7.2	157
	24.8	1.3	9.6	0.12	9.9	3.2			
2	22.5	1.2	14.0	0.15	14.3	3.8	1.2	6.2	157
	23.9	1.4	9.0	0.11	10.2	3.2			
3	23.2	1.2	21.0	0.24	21.9	4.7	1.8	7.4	167
	24.9	1.2	7.2	0.08	6.8	2.6			
4	23.0	1.2	18.4	0.20	18.8	4.3	1.6	6.6	157
	24.2	1.4	6.4	0.08	7.0	2.6			
5	22.7	1.2	15.8	0.17	16.0	4.0	1.2	6.7	160
	24.4	1.4	9.2	0.12	10.3	3.2			

[a] The position ($\bar{\nu}$) and half-width (δ) in kK of each peak of maximum extinction ϵ_{max} (10^3 cm^{-1} M^{-1}). [b] The oscillator strength (f), dipole strength ($D \times 10^{-36}$ cgsu), transition moment ($\rho \times 10^{-18}$ cgsu), and the ratio of these moments for the peaks (ρ_1/ρ_2). [c] Total area accounted for by the analysis (10^4 kK cm^{-1} M^{-1}). The experimental area is 7.1×10^4 kK cm^{-1} M^{-1} and was determined by planimetry. [d] Standard deviation in extinction units.

Table V. Peak Parameters for the Visible Spectrum of the Ligand 1-(2'-Pyridyl)-3-(6''-methyl-2''-pyridyl)-1,2-diaza-2-propene, Obtained by Gauss–Newton Nonlinear Analysis: One- and Three-Peak Analysis[a]

No. of peaks	$\bar{\nu}$, kK	δ, kK	ϵ_{max}, cm^{-1} M^{-1}	SD
1	23.2	1.5	20.3	983
1	23.2	1.5	20.2	983
3	22.1	1.0	8.2	
	23.0	0.9	10.6	130
	24.4	1.3	10.0	
3	22.1	1.0	8.6	
	23.0	0.9	10.6	138
	24.4	1.3	10.1	

[a] Symbols as defined in Table IV.

will be more stabilized relative to them by high dielectric solvents.

Finally, the calculation of the transition dipole moments by HMO theory, in general, supports the above assignments of $\vec{\rho}_1$ and $\vec{\rho}_2$. The energies of the various transitions shown in Table II were calculated by normalizing the $\pi_8 \rightarrow \pi_9$ transition energy to the lower energy obtained from the GN analysis.

The visible and CD spectra of complexes I and II are shown in Figures 6 and 7. The spectra are remarkably similar; the total integrated intensity in the visible spectra is about twice that of the free ligand, while that of the CD spectra is close to zero, a gratifying fulfillment of the requirements for using the exciton method. The visible spectra were subjected to GN analysis, assuming the presence of three and four peaks. The results are summarized in Table VI. Of the four theoretical transitions, one ($A_0 \rightarrow A_+$) has an almost negligible dipole strength (Table III). The GN analysis agrees with this result—the three-peak analysis accounts for most of the envelope, while the introduction of the fourth peak absorbs the small error into a small peak, without significant change in the other three.

Structure of the Complexes. Figure 1 shows the idealized geometry of the free ligand. This geometry is probably distorted in the complexes. Placing the donor atom N2 axially with respect to the metal ion at a distance of 2 Å generates N1–M and N4–M distances of 2.5 Å. These distances can be shortened by allowing the C6–N2–N3 bond angle to open symmetrically from 120° in the idealized structure to 130 and 140°; the resulting bond lengths are 2.2 and 2.1 Å, respectively.

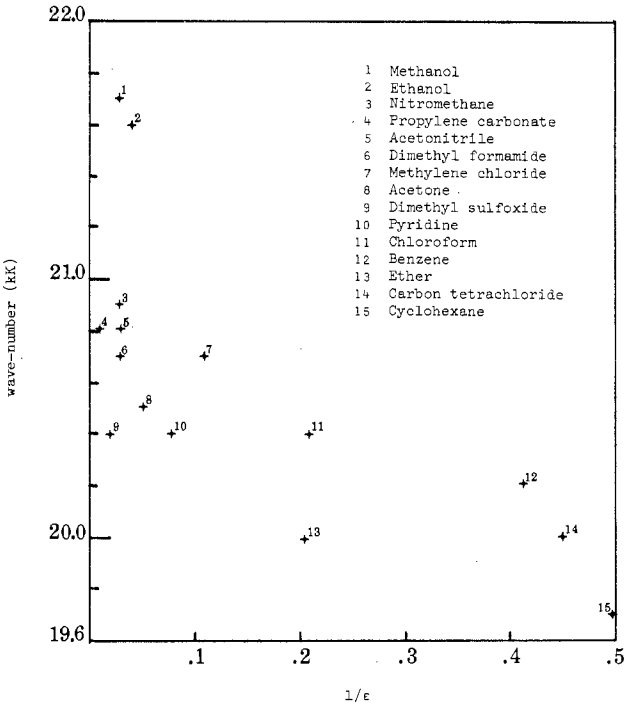

Figure 5. Wave number of the absorption maxima of solutions of complex I plotted against the reciprocal of the dielectric constant of the solvents.

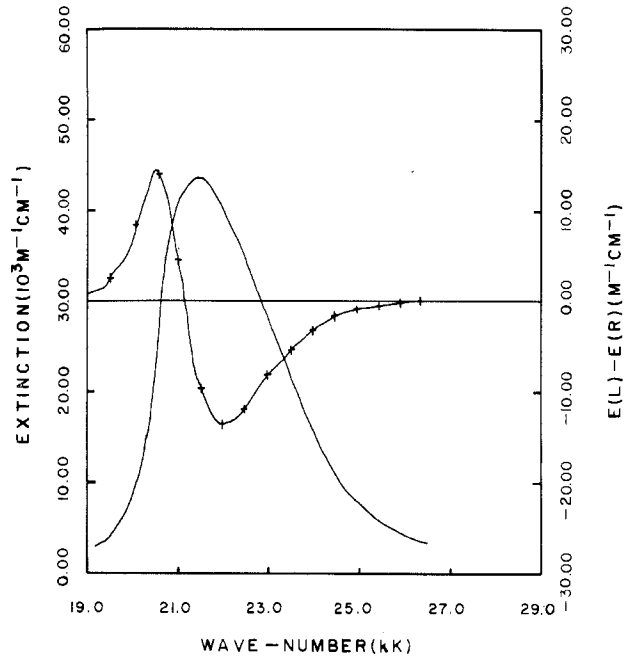

Figure 6. The visible spectrum (solid line) and CD spectrum (crossed line) of the nickel complex I.

The directions of the transition dipole moments are affected by this tetragonal compression and two angle factors, θ_1 and θ_2 of Figure 2, take account of this in the calculation of the theoretical results.

Approximations in the Exciton Method. Several approximations have been made in using exciton theory to predict the absolute configuration of complexes I and II. The Hamiltonian for the system should be written more correctly as $\hat{h}_c = \hat{h}_x + \hat{h}_y + \hat{h}_m + V_{xy} + V_{my} + V_{mx}$, where ligand-metal interactions and the free metal Hamiltonian are included. The suppression of the terms V_{mx} and V_{my} and of the matrix elements $H\Phi_{12}$ involves some drastic ap-

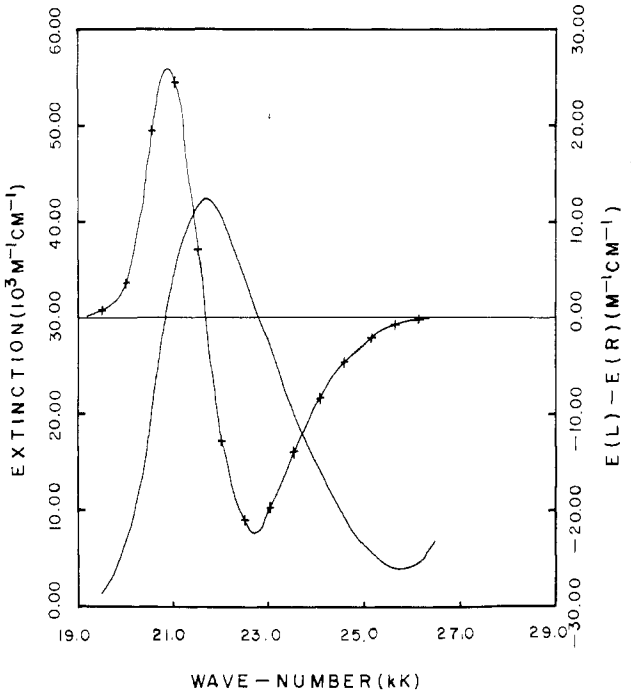

Figure 7. The visible spectrum (solid line) and CD spectrum (crossed line) of the zinc complex II.

Table VI. Peak Parameters for the Visible Spectra of Complexes I and II, Obtained by Gauss-Newton Nonlinear Analysis: Three- and Four-Peak Analyses[a]

Data set[b]	$\bar{\nu}$	δ	ϵ_{max}	f	D	ρ	SD
1	21.2	0.79	31.8	0.23	23.3	4.8	
	22.6	0.86	17.2	0.14	12.8	3.6	244
	23.3	1.94	13.5	0.24	22.0	4.7	
	22.1	0.53	2.9	0.01	1.3	1.1	
2	21.2	0.70	26.9	0.17	17.2	4.2	
	22.4	0.72	16.8	0.11	10.5	3.2	187
	23.0	1.72	17.9	0.28	26.2	5.1	
	22.0	0.35	3.3	0.01	1.0	1.0	
3	21.3	0.79	26.2	0.19	18.9	4.4	337
	22.3	0.74	9.4	0.06	6.1	2.5	
	22.7	1.77	22.9	0.37	34.9	5.9	
4	21.2	0.79	27.7	0.20	20.2	4.5	330
	22.3	0.91	25.4	0.21	20.3	4.5	
	23.7	1.32	13.6	0.16	14.8	3.8	

[a] Symbols as defined in Table IV. [b] Data sets 1 and 3 are the results of the analysis for the nickel complex; 2 and 4 are those for the zinc complex.

proximations. Matrix elements of the form $\langle X_i M_0 | V_{mx} | X_j M_0 \rangle$ take account of the Coulomb interaction between the ligand density functions $|X_i X_j\rangle$ and the metal ion. It has been assumed in previous work that the metal ion stabilizes all ligand states to the same extent.[10] This is a poor assumption even when the ligand is a neutral one like 1,10-phenanthroline or 2,2′-bipyridine. Here, the ligand bears a negative charge that is closer to the metal ion in excited states than in the ground state. Clearly, the ground state of the ligand is less stabilized than the excited states, resulting in a red shift for the ligand transitions upon complexation. This alone can account for the 1-kK difference between observed and calculated transitions.

Metal ion stabilization will, in general, be different for the various energy levels of the complex; this result can have a profound effect on the calculated CD spectrum and questions the ordering of states, thus jeopardizing the assignment of absolute configuration. The excellent agreement, apart from the 1-kK red shift, between calculated and observed properties suggests that no change in the ordering of states has occurred. Interchange of the A_- and B_- energy levels produces spectra totally different from those observed.

Setting $H\Phi_{12}$ equal to zero is much less a sin of omission. Again, the justification of ignoring this interaction is the excellent agreement of the calculated and observed results.

Theoretical Spectra. The theoretical visible and CD spectra of the complexes were obtained as follows. The calculated dipole and rotational strengths were related to extinction coefficients through the equations

$$D = 91.8 \times 10^{-40} \int \{\epsilon(\nu)/\bar{\nu}\}\, d\bar{\nu}$$

$$R = 22.9 \times 10^{-40} \int \{\epsilon_l(\bar{\nu}) - \epsilon_r(\bar{\nu}))/\bar{\nu}\}\, d\bar{\nu}$$

By assuming gaussian line shapes these reduce to

$$D = 91.8 \times 10^{-40} \sqrt{\frac{\pi}{\ln 2}} \epsilon_{max} \delta / \bar{\nu}_{max}$$

with a similar expression for the rotational strength. The calculated values for D, R, and $\bar{\nu}_{max}$ and the empirical value of δ (the half-width obtained from GN analysis of the observed spectra) were then used to calculate ϵ_{max} and $(\epsilon_l - \epsilon_r)_{max}$ for each peak. The envelopes were calculated from the gaussian line shape and added to give simulated visible and CD spectra.

Two sets of the calculated values for ϵ_{max} and $(\epsilon_l - \epsilon_r)_{max}$ for each transition are shown in Table III. The first set corresponds to half-width data set 1 (Table VI), obtained from GN analysis of the nickel complex's spectrum, and the second to data set 2, from the zinc complex's spectrum. For the purpose of simulating the CD spectra, we have assumed that the half-widths associated with the absorption of left and right circularly polarized light are identical.

The simulated curves, showing best agreement with the observed curves, are shown in Figure 8.

Experimental Section

Spectra. Optical rotatory dispersion and circular dichroism spectra were obtained using a JASCO ORD/UV-5/CD-1 spectropolarimeter. The sample cells for both ORD and CD measurements were 1-cm cylindrical fused-quartz absorption cells made by the Pyrocell Manufacturing Co., Inc. The cells showed uniform rotation of no more than ±0.001° over the range 700–400 nm. Ultraviolet and visible spectra were recorded on a Cary Model 14 spectrophotometer.

Computational Procedure. All programs were written in these laboratories in double precision PL/I. The calculations were carried out on an IBM 360-50 computer.

Gauss-Newton Nonlinear Analysis.[19] Assuming the presence of n component peaks, the spectrum is synthesized from initial guesses for the parameters ϵ_0, δ, and $\bar{\nu}_0$ associated with each peak. The synthesis is subjected to least-squares constraints with the parameters being varied until the standard deviation approaches some chosen small value. This best set of parameters is then used as the initial guesses for a Gauss-Newton nonlinear least-squares analysis,[19] the calculation being iterative. Each set of corrections obtained from the analysis is subjected to Box's modification to improve convergence.[20]

Materials. (*RS*)-Bis[1-(2′-pyridyl)-3-(6″-methyl-2″-pyridyl)-1,2-diaza-2-propene]nickel(II) perchlorate (III), (*RS*)-bis[1-(2′-pyridyl)-3-(6″-methyl-2″-pyridyl)-1,2-diaza-2-propene]zinc(II) perchlorate (IV), (*RS*)-bis[1-(2′-pyridyl)-3-(6″-methyl-2″-pyridyl)-1,2-diaza-2-propenato]nickel(II) (I), and (*RS*)-bis[1-(2′-pyridyl)-3-(6″-methyl-2″-pyridyl)-1,2-diaza-2-propenato]zinc(II) (II) were prepared by previously described methods.[21] Potassium antimonyl tartrate was purchased from Baker and Adamson Chemical Co. All compounds were characterized, when necessary, by analyses

(19) K. L. Nielsen "Methods in Numerical Analysis," 2nd ed, Macmillan, New York, N. Y., 1964, p 308.
(20) G. E. P. Box, *Bull. Inst. Int. Statist.*, 36, 215 (1958).
(21) J. F. Geldard and F. Lions, *Inorg. Chem.*, 2, 270 (1963).

carried out at Galbraith Laboratories, Inc., Knoxville, Tenn.

Resolutions. (*S*)-Bis[1-(2′-pyridyl)-3-(6″-methyl-2″-pyridyl)-1,2-diaza-2-propenato]benzenenickel(II) (I-S). Ethanolic solutions of the *RS* complex III (1 molecular proportion) and potassium antimonyl tartrate (1 molecular proportion) were mixed at 75° and cooled slowly to 40°. Crystallization of the less soluble diastereoisomer was induced by prolonged scratching of the wall of the reaction flask with a glass rod. The solution was then cooled to room temperature and the crystals were collected and washed with ice-cold water. The crystals were repeatedly recrystallized until a maximum and constant rotation at a pertinent wavelength was obtained; then they were converted by treatment with base to I-S.[21] *Anal.* Calcd for $NiC_{30}H_{28}N_8$: C, 64.5; H, 5.0. Found: C, 64.3, H, 5.1.

The clear filtrate from above was allowed to stand in an ice bath for 2 hr to allow crystallization of the less soluble diastereoisomer. The crystals were collected and recrystallized to constant rotation. No further use was made of this material.

The experimental spectra described in this paper are those of I-S; no racemization of I-S in solution was observed.

(*S*)-Bis[1-(2′-pyridyl)-3-(6″-methyl-2″-pyridyl)-1,2-diaza-2-propene]zinc(II) Antimonyl Tartrate (V-S). Ethanolic solutions of *RS* complex IV and potassium antimonyl tartrate were admixed as above. Yellow crystals separated immediately; these were collected by filtration of the hot solution and washed well with ice-cold ethanol. This material was not recrystallized but used as prepared to generate II-S in solution (see below).

CD Spectrum of *S*-Bis[1-(2′-pyridyl)-3-(6″-methyl-2″-pyridyl)-1,2-diaza-2-propenato]zinc(II) (II-S). The complex V-S was dissolved in absolute ethanol made basic with solid sodium hydroxide, thus generating a solution of II-S. The circular dichroism spectrum of this solution was recorded, no racemization of the complex being observed during this time. The concentration of II-S was determined spectrophotometrically using the optical density at 21.74 kK.

The CD and visible spectra of I-S and II-S are shown in Figures 6 and 7, respectively.

Conclusion

The use of the exciton theory for calculation of the visible and CD spectra of the nickel(II) and zinc(II) complexes, I and II, respectively, gives results in good qualitative agreement with the observed spectra. The quantitative error in line position is believed mostly due to the difference between ligand ground- and excited-state interaction with the metal ion.

Based on the above results, however, the enantiomers of the nickel(II) and zinc(II) complexes, whose visible and CD spectra are shown in Figures 6 and 7, respectively, must be assigned an absolute configuration enantiomeric to that represented in Figure 2 and thus must be assigned the designation *S*.

Registry No. I, 37897-29-3; II, 37861-96-4.

Appendix

The absolute configuration of the complex represented in Figure 2 has been designated *R*. This designation obtains from the following considerations.

(a) The ligand planes in the complex define a right-handed helix with respect to the C_2 axis.

(b) The Newman projection of the complex, shown below, is analogous to that of the biphenyl system. Application of the rules of Cahn, Ingold, and Prelog[22] leads to the assignment *R* for this configuration. Omitting the methyl groups in this projection does not alter the assignment.

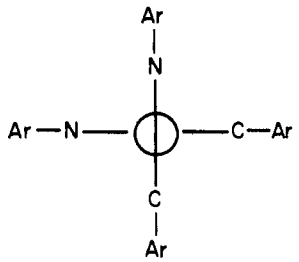

(c) The rules of Hawkins and Larsen[23] give no result unless one considers only the positions of like halves of the ligands. In this case, the symbol *R* would be assigned to the structure.

(d) The tentative rules suggested by the Commission on the Nomenclature of Inorganic chemistry of the IUPAC[24] have been ignored because again one can only consider like halves of the ligands. Their relative position has been designated Λ by these rules.

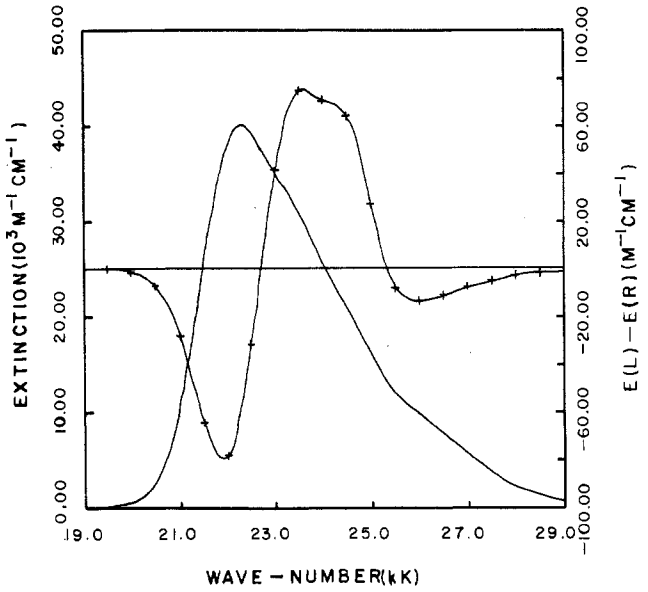

Figure 8. The calculated visible spectrum (solid line) and CD spectrum (crossed line) of the complex shown in Figure 2. The curves correspond to the information given for the nickel complex in data set 10 of Table III.

(22) R. S. Cahn, C. K. Ingold, and V. Prelog, *Angew. Chem.*, 78, 413 (1966); *J. Org. Chem.*, 35, 2849 (1970).

(23) C. J. Hawkins and E. Larsen, *Acta Chem. Scand.*, 19, 185 (1965).

(24) *Inorg. Chem.*, 9, 1 (1970).